ISSN 1068-3755, Surface Engineering and Applied Electrochemistry, 2015, Vol. 51, No. 4, pp. 394–400. © Allerton Press, Inc., 2015.

Effects of Different Treatment of TiO_2 Electrodes on Photovoltaic Characteristics of Dye-Sensitized Solar Cells[1]

Qi-Bin Lin[a], Li-Wei Wang[b], and Shi-Hua Huang[b]

[a] *The School of Electronic and Electrical Engineering, Chuzhou University, Anhui, 23900 China*

[b] *Department of Physics, Zhejiang Normal University, Zhejiang, 321004 China*

e-mail: qibinlin@126.com

Received February 6, 2015

Abstract—Using the pre-treatment of the working photoelectrode and the admixture light-scattering layer can ameliorate the performance of TiO_2 dye-sensitized solar cells (DSSCs). $TiCl_4$ treatments on TiO_2 electrodes improve the adhesion and mechanical strength of the TiO_2 layer. The HNO_3 treatment significantly enhances the dispersion of TiO_2 particles and increases the surface area and porosity of TiO_2 films. The scattering layer formed by admixing both nanometer-sized and submicron-sized TiO_2 particles greatly enhances the DSSC performance. The light absorption is considerably better in TiO_2 films with a mixture of large and small particles. This mixture is capable of efficient light-scattering while simultaneously providing a larger surface area for effective dye adsorption. Each of these technologies for the TiO_2 film fabrication has a significant influence on the overall photovoltaic parameters of DSSCs, resulting in improvements in energy conversion performance.

Keywords: dye-sensitized solar cells, $TiCl_4$ treatment, HNO_3 treatment, submicron-sized TiO_2, scattering layers

DOI: 10.3103/S1068375515040109

INTRODUCTION

Dye-sensitized solar cells (DSSCs) designed by Grätzel and O'Regan in 1991 show great promise as a cost-effective alternative to traditional *p–n* junction solar cells [1–3]. In order to enhance photovoltaic conversion efficiency, much research has been focused on searching for new dye-sensitizers, suppressing charge recombination, improving interfacial interaction and modifying electrolyte components [4]. In order to bring the modules to the market, minimum usage of the photoactive dye is taken into account since the cost of the dye is still higher relative to other components in the module. Thin TiO_2 films with a larger surface area and better light scattering abilities are an essential requirement for the production of DSSC modules, thus the mitigation of the production cost due to reduced dye use would be feasible without sacrificing photovoltaic performances. A larger surface area is usually obtained with smaller particle sizes, however, poor light scattering. A very important aspect in the production of highly efficient DSSCs is the technique of reformation of a porous nanocrystalline TiO_2 film. Recently, an improvement in the light harvest efficiency has been achieved: a submicron crystalline light-scattering layer was deposited on a transparent nanocrystalline TiO_2 film [5–8]. The presence of the scattering layers with large particles can induce sufficient light trapping in DSSCs due to the increase of the absorption path length of photons and optical confinement. This length can be larger than the thickness of the film if the light is scattered within it or if it is reflected at the back of the cell. It is desirable to enhance the absorption of light by the cell for a given dye and film thickness. The introduction of these submicron particles will unavoidably reduce the internal surface area of the photoelectrode film, and the dye adsorption is expected to be much lower for these particles than for the nanocrystalline TiO_2, which counteracts the enhancement effect of light-scattering on optical absorption. Computer simulation results indicate that light absorption is enhanced substantially in the nanocrystalline film with a binary mixture of large and small particles. This mixture is capable of efficient light-scattering while simultaneously providing a larger surface area for an effective dye adsorption [9].

In classical nanoparticulate DSSCs, a titanium tetrachloride ($TiCl_4$) treatment is usually used to improve solar cell efficiency [10, 11]. The $TiCl_4$ pre- and post-treatments refer to the treatment of the fluorinated tin oxide (FTO) covered glass and the TiO_2 film with an aqueous solution of $TiCl_4$, respectively. Pre-treatment greatly influences the bonding strength between the FTO substrate and the porous TiO_2 film and hinders

---

[1] The article is published in the original.

the charge recombination between injected electrons and I_3^- ions [12]. The $TiCl_4$ post-treatment enhances the surface roughness factor and the electrical contact between the TiO_2 particles, thus improving dye adsorption and resulting in a higher photocurrent [12]. However, the hypothesis explaining an increment in the photocurrent remains controversial. O'Regan et al. [13] reported that the contribution of $TiCl_4$ post-treatment lowers the TiO_2 conduction band edge potential and decreases the electron recombination rate constant, resulting in the increase in quantum efficiency of charge separation at the interface. The results of the Raman spectra of DSSCs post-treated with $TiCl_4$ indicated new rutile layers on the TiO2 surface, resulting in the epitaxial growth of new layers on the electrode surface consisting entirely of rutile nanoparticles [14]. Therefore, the effects of the $TiCl_4$-treated TiO_2 electrodes on the photovoltaic properties of DSSCs have not been fully elucidated. On the other hand, the acid treatment of the TiO_2 surface has been shown to improve the photoelectric performance of DSSCs [15–17]. This behavior is ascribed to the protonation effect that promotes dye adsorption and hinders the charge recombination between injected electrons and I_3^- ions. However, Hao et al. [18] reported on the decrease of the photocurrent and efficiency of acid-treated DSSCs. These inconsistencies indicate that the influences of an acid-treated TiO_2 electrode on the photovoltaic performances of DSSCs need further clarification. In order to better understand those effects, the surface states of both the acid-treated and $TiCl_4$-treated TiO_2 film should also be investigated.

This article describes the photovoltaic characteristics of DSSCs fabricated using multi-layered, $TiCl_4$-treated and acid-treated TiO_2 electrodes. Also, the influences of various technical procedures on the photovoltaic performance of highly efficient DSSCs are investigated by studying the morphological changes, crystalline phase, ultraviolet and visible (UV-Vis) absorption characteristics and surface states of TiO_2 particles, as well as the photocurrent-voltage (I–V) characteristics of the cells.

EXPERIMENTAL DETAILS

Materials

Electrodes were fluorine-doped tin oxide coated glass substrates: $F:SnO_2$ or FTO, size ~2 cm × 2 cm, sheet resistivity ~15 Ohm/mm^2, light transmissivity ≥90%. $TiCl_4$ was diluted with deionized water to 2 M at 5°C to make a stock solution, and was kept in a freezer. Commonly used chemical reagents were tetraisopropyl titanate, chloroplatinic acid, terpineol, ethyl cellulose, isopropyl alcohol, polyethylene glycol (PEG, $M_w = 20000$), absolute ethyl alcohol, acetone, acetylacetone, acetonitrile, BMII (1-butyl-3-methyl imidazole iodized salt), guanidinium isothiocyanate, 4-*tert*-butylpyridine, iodine (I_2). All of the solvents and chemicals employed for the experiments were of reagent or spectrophotometric grade. The redox electrolyte used here is a solution of 0.6 M BMII, 0.03 M I_2, 0.1 M guanidinium thiocyanate, and 0.5 M 4-*tert*-butylpridine in a mixture of acetonitrile and valeronitrile. N719 dye (bis(isothiocyanato)bis(2,2'-bipyridyl-4,4'-dicarboxylato)-ruthenium(II)-bis-tetrabutyl ammonium). A Ti-precursor solution was formed by adding 10 mL tetraisopropyl titanate and 1.5 mL acetylacetone to 10 mL absolute ethanol.

Preparation of TiO_2 Colloids with Nano Particles and Submicroparticles

In the modified hydrothermal method, a mixture of 7.1 g tetraisopropyl titanate and 1.5 g acetic anhydride was added dropwise into 36.5 mL deionized water. After stirring for about 1 h, 0.5 mL of the concentrated nitric acid was added dropwise to the mixture solution, the solution was then heated to 80°C and peptized for 75 min under ultrasonic vibration. In order to accomplish a complete hydrolysis reaction, more than one hour of stirring was needed. After cooling down, the mixture was diluted with deionized water to a final 46.5 mL. The resulting gelatin was loaded into a titanium autoclave and heated at 230°C for 24 h. Subsequently, the obtained suspension-containing precipitate was diluted with absolute ethanol to 100 mL and thoroughly dispersed under ultrasonic vibration at atmospheric conditions until a homogenously dispersed and stable colloid appeared.

The synthesis of submicron TiO_2 particles in a base solution was different from that in an acid solution. The mixture of 7.1 g (0.025 M) titanium isopropoxide and 1.5 g (0.025 M) isopropyl alcohol was formed under ultrasonic vibration at atmospheric conditions for about 30 min. Then 14.5 mL deionized water was added to this mixture as quickly as possible and stirred for 1 h. A white precipitate was obtained using a centrifuge and washed several times with deionized water. After the dropwise addition of 3 mL of 0.6 M tetramethylammonium hydroxide (TMAH), the precipitate was enclosed in a titanium autoclave and heated at 230°C for 12 h. The resultant solution was treated using the same method as with the acidic solution.

Preparation of Screen-Printing Pastes

Into 2 g pure TiO_2, obtained from the previously prepared precipitate, 1.1 g ethyl cellulose (EC) (10 wt % ethanolic solution) and 6.8 g of terpineol (60 wt % ethanolic solution) were added. This mixture was diluted with ethanol to obtain a final total volume of ~60 mL and was then sonicated with hand stirring. Ethanol and water were removed from these TiO_2/ethyl cellulose solutions by a blast oven. The final screen-printing

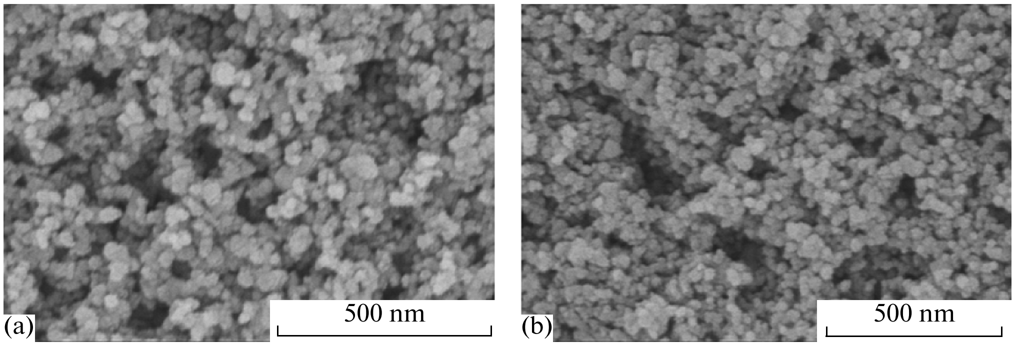

Fig. 1. SEM images of TiO_2 films untreated (a) and after $TiCl_4$ treatment (b).

pastes correspond to 20 wt % TiO_2, 11 wt % ethyl cellulose and 69 wt % terpineol (paste *A*). For the paste used in the light-scattering layers (paste *B*), TiO_2 nanoparticles were mixed with submicron TiO_2 particles to give a final paste formulation of 22% submicron-sized TiO_2, 70% nanometer-sized TiO_2 and 8% ethyl cellulose in terpineol.

Preparation of Porous-TiO_2 Electrodes

The characteristics of the screen used here are as follows: material, polyester; mesh count, 80T mesh/cm; mesh opening, 45 μm; thread diameter, 60 μm; open surface, 29.8%; fabric thickness, 78 μm. The FTO glass was first cleaned in a detergent solution and then rinsed with water and ethanol. The FTO glass plates were immersed into a 40 mM aqueous $TiCl_4$ solution at 80°C for 30 min and washed with water and ethanol. Before screen-printing, TiO_2 pastes A and B were acid-treated by stirring in 1 M HNO_3 aqueous solution at 80°C for 3 h and dried 100°C for 8 h. A layer of paste A was coated on the FTO glass plates by screen-printing and then dried for 3 min at 115°C. Subsequently, two layers of paste B were printed at about ~4 μm as a light-scattering layer. The electrodes coated with the TiO_2 film were sintered under an airflow at 450°C for 30 min, then treated with a 40 mM aqueous $TiCl_4$ solution at 80°C for 30 min, after that washed with water and ethanol and sintered at 500°C for 30 min. After cooling to a temperature of 80°C, to avoid water adsorption through capillary effects, the electrode was immerged in a 0.5 mM N-719 dye solution for sensitizer impregnation and kept at room temperature for 24 h.

Assembling of DSSCs

The TiO_2 work electrode covered with dye was assembled and sealed with a hot-melt gasket of 20 μm thickness made of ionomer resin. A drop of electrolyte was put on the film in the back of the counter electrode. It was introduced into the cells via vacuum backfilling. The cells were placed in a small vacuum chamber to remove inner air. Exposing the electrolyte again to ambient pressure causes it to be driven into the cells. Finally, the hole was sealed using a hot-melt gasket film and a cover glass.

Characterization and Photovoltaic Measurement

The morphology of scattering particles was investigated by a field-emission scanning electron microscope. The X-ray diffraction (XRD) data were obtained using a diffractometer. Absorption spectra were measured using a UV-Vis spectrophotometer equipped with an integrating sphere. The Fourier transform infrared (FTIR) absorption spectra were measured by a spectrometer within a range 400–4000 cm^{-1}. The photovoltaic measurements utilized a 150 W xenon lamp. The power of the simulated light was calibrated to 100 mW/cm^2 (AM 1.5) using a reference Si photodiode. The I–V characteristics were measured by a digital source meter and controlled automatically by a computer.

RESULTS AND DISCUSSION

$TiCl_4$ and HNO_3 Treatments

Figure 1 shows the SEM surface images of the untreated and $TiCl_4$-treated TiO_2 films. Compared with the untreated film, the $TiCl_4$-treated TiO_2 film shows small aggregates, relatively good surface coverage, and an improvement in particle necking. The $TiCl_4$ pre-treatment on TiO_2 working electrodes enhances the bonding strength between the FTO substrate and the porous TiO_2 layer and blocks the charge recombination between electrons originated from the FTO and the I_3^- ions in the I^-/I_3^- redox couple. The $TiCl_4$ post-treatment enhances the surface roughness factor and necking of TiO_2 particles, resulting in an increase of dye adsorption and higher photocurrent.

The $TiCl_4$ treatment has a great influence on the TiO_2 rutile phase, as shown in Fig. 2. For an untreated TiO_2 film, an obvious XRD peak located at 27.5° can be observed, which is attributed to the TiO_2 rutile-phase. After the $TiCl_4$ pre-treatment on the TiO_2

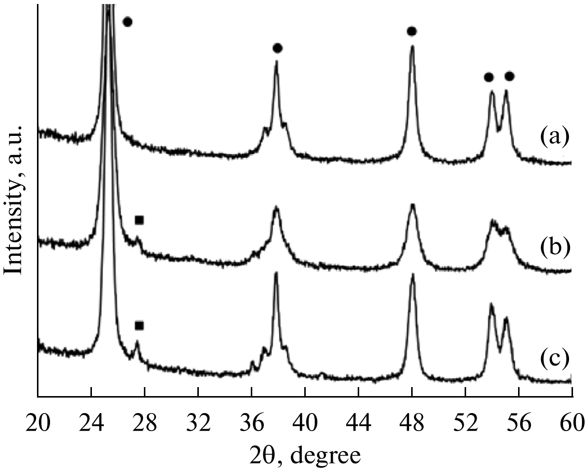

Fig. 2. XRD spectra of TiO_2 film untreated (a) and with $TiCl_4$ pre-treatment (b) and post-treatment (c). The patterns "■", "●" denote peaks for rutile phase and anatase phase, respectively.

working electrode, the intensity of this peak decreases. This TiO_2 rutile phase is not present after the $TiCl_4$ post-treatment. At room temperature TiO_2 has two phases, i.e., rutile and anatase. The anatase phase has a more open structure than the rutile phase [19]. Therefore, a pure anatase phase is preferred to achieve a larger surface area necessary to obtain a higher photocurrent. The titanium complexes present in the $TiCl_4$ solution condense at the interpart of the film, which results in an epitaxial growth of new layers on the TiO_2 electrode surface consisting of anatase nanoparticles. This epitaxial growth enhances the necking of the TiO_2 particles, which may result from the phase transformation of a few TiO_2 nanoparticles from rutile to anatase [10].

Figure 3 shows SEM images of the untreated and HNO_3-treated TiO_2 films. The dispersion of TiO_2 particles is significantly increased by the acid treatment, which results in the HNO_3-treated TiO_2 particles being protonated and positively charged by the adsorbed HNO_3 [15, 16]. The electrostatic attraction between the positively charged TiO_2 surface and the negatively charged end of the dye molecules can also assist dye adsorption. The HNO_3-treated TiO_2 film exhibited higher porosity and larger pore sizes, while the untreated TiO_2 film showed larger particle aggregations. Compared with the untreated TiO_2 film, the HNO_3-treated TiO_2 film possesses larger porosity and pore size. With the increase of the surface area and number of appropriate pores in the TiO_2 film, the dye adsorption increases and the electron transfer in a redox electrolyte becomes easier.

The surface of the HNO_3-treated TiO_2 film was investigated using FTIR measurements. Figure 4 shows FTIR spectra of both untreated and HNO_3-treated TiO_2 films. For the HNO_3-treated TiO_2 film, the peak located at 1650 cm^{-1} was observed, which is ascribed to an H–O–H bending mode. This result indicates that the TiO_2 nanoparticle surface is hydroxylated and protonated during the acid treatment. The HNO_3-treated TiO_2 film exhibits a sharp and intense peak at 1380 cm^{-1}, which is due to the presence of an NO_3^- group [20]. We consider the coverage of NO_3^- ions on the TiO_2 surface to block the path of the electron backward transfer, resulting in the improvement of the DSSC conversion efficiency.

The $TiCl_4$ treatment on the TiO_2 film induces a decrease of TiO_2 band gaps [21], which results in enhancing the electron injection efficiency. As shown in Fig. 5, a short-circuit current (J_{sc}) of the $TiCl_4$ treated DSSCs increases with respect to untreated DSSCs. For DSSCs with $TiCl_4$-treatment, a slight decrease in the open-circuit voltage (V_{oc}) is contributed to the downward shift of the quasi-Fermi level. Nonetheless, the photoelectric conversion efficiency of DSSCs with $TiCl_4$-treatment film obviously increases, compared to that of the untreated TiO_2 film. As seen from Fig. 5, the J_{sc} and V_{oc} increased due to the HNO_3 treatment. The J_{sc} increment in the HNO_3 treatment of TiO_2 is ascribed to a higher charge collec-

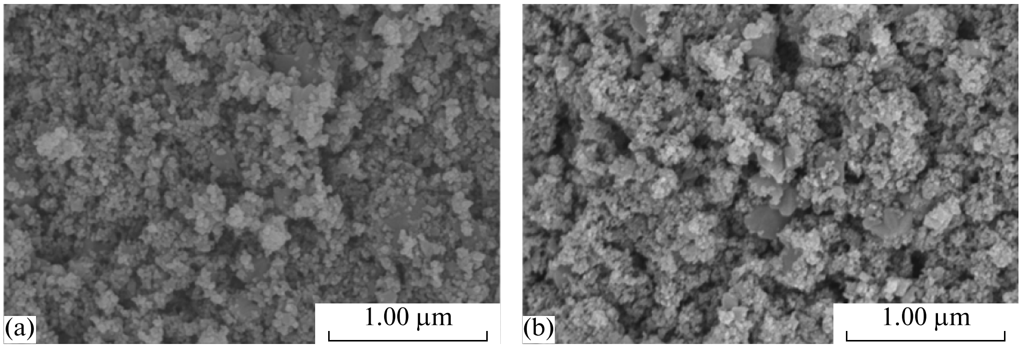

Fig. 3. SEM images of TiO_2 films untreated (a) and after HNO3 treatment (b).

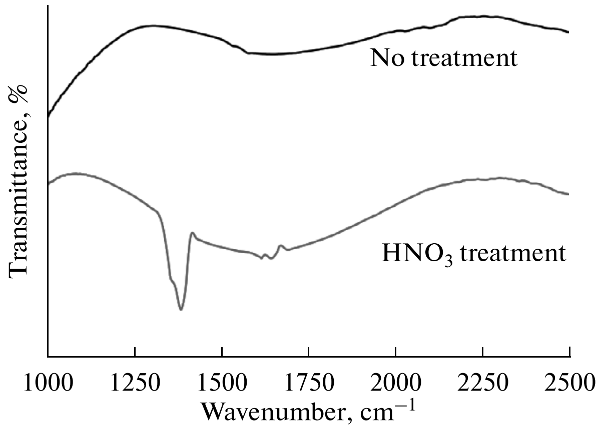

Fig. 4. FTIR spectra of untreated and HNO_3-treated TiO_2 films.

tion efficiency by the surface protonation of TiO_2 and the retarded backward electron transfer by anion (NO_3^-) adsorption on the TiO_2 surface [22]. Theoretically speaking, V_{oc} is the potential difference between the Fermi level of TiO_2 and the reversible redox couple (I^-/I_3^-) in the electrolyte. After HNO_3 treatment, the V_{oc} increment may be caused by the shift of the flat band potential of TiO_2 in a positive direction. A positive shift of the flat band potential has been reportedly observed when TiO_2 was acid-treated due to the adsorption of H^+ ions on the TiO_2 surface [23].

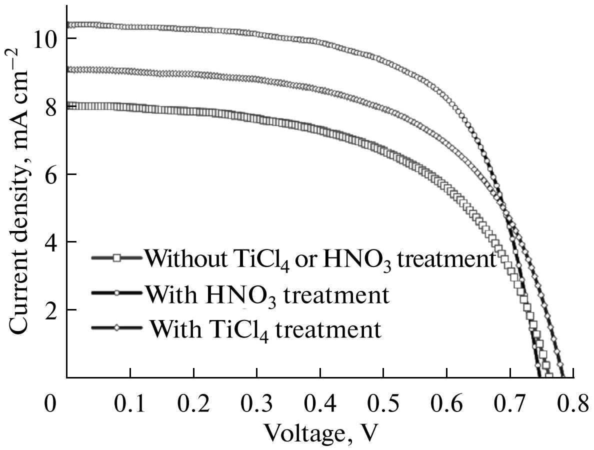

Fig. 5. Photovoltaic performance of DSSC devices using TiO_2 electrodes with and without $TiCl_4$ or HNO_3 treatments under light density: 100 mW/cm^2; AM 1.5, active area: 0.36 cm^2.

Effect of Light-Scattering TiO_2 Layer

Figure 6 shows SEM images of TiO_2 films with differently sized scattering particles, G1, G2 and G3. The average sizes of G1 and G2 are estimated to be about 30 and 250 nm, respectively, while G3 particles are a mixture of G1 and G2 particles with a mixing ratio of G1 : G2 ~ 4 : 1. Nanometer-sized G1 particles are mostly revealed as sphere-shaped, and submicron-size G2 particles as mostly hexagonally-shaped. Furthermore, the SEM images demonstrate that the films had a porous structure, propitious to adsorb much more dye molecules than a compact structure. Figure 7 shows a UV-Vis absorption spectra of four types of TiO_2 films with dye sensitization, where the letters “N”, “S” and “M” denote a nanometer-size TiO_2 layer, a submicron-size TiO_2 layer, and a mixture of submicron- and nanometer-size TiO_2 layer, respectively. All of the dye-sensitized TiO_2 films with different structures exhibit almost similar absorption intensities below 350 nm. This effect is caused by the intrinsic absorption of TiO_2 semiconductors that incident light with a photon energy larger than a TiO_2 band gap can be absorbed by TiO_2 film. However, the absorption for light wavelengths more than 350 nm is significantly different, which results from the dye molecules adsorbed on the TiO_2 surface and the film structure.

Photovoltaic performance of DSSC devices based on four types of TiO_2 films under light density: 100 mW/cm^2; AM 1.5, active area: 0.36 cm^2

Type of structure	J_{sc} (mA/cm^2)	V_{oc} (V)	Fill factor	Efficiency (%)
M/N/FTO	15.5	0.71	0.65	7.2
S/N/FTO	14.1	0.68	0.64	6.1
N/FTO	12.3	0.70	0.66	5.7
S/FTO	10.8	0.61	0.54	3.6

As seen in Fig. 7, the highest integrated absorption intensity is for M/N/FTO, slightly less intense for S/N/FTO, and the lowest intensity is exhibited for S/FTO. It should be noted that S/FTO shows the lowest absorption intensity as the light wavelength (λ) varies from 300 to 670 nm. Larger TiO_2 particles have a smaller internal surface area, which results in less dye adsorption. Therefore, the absorption of submicron-sized TiO_2 particles is the lowest for $\lambda = 300\text{~}670$ nm. However, its absorption is larger than that of N/FTO and S/N/FTO for wavelengths over 670 nm, which may be mainly due to high back-scattering. As shown in Fig. 7, a mixture structure with an admixture of about 20% 30-nm particles and about 80% 250-nm particles has the highest integrated absorption intensity. This induces more effective light capturing in the visible spectrum and has a strong light-scattering effect. If there are too many large particles, not only does the effective internal surface decrease, but also there is too much back-scattering. In this case, the reflectance of the cell is enhanced, not its absorptance.

The photovoltaic characteristic of the DSSCs constructed with different types of TiO_2 electrodes under AM 1.5 illumination are summarized in the table. For the TiO_2 scattering layer with an admixture of 30-nm particles and 250-nm particles (M/N/FTO), the pho-

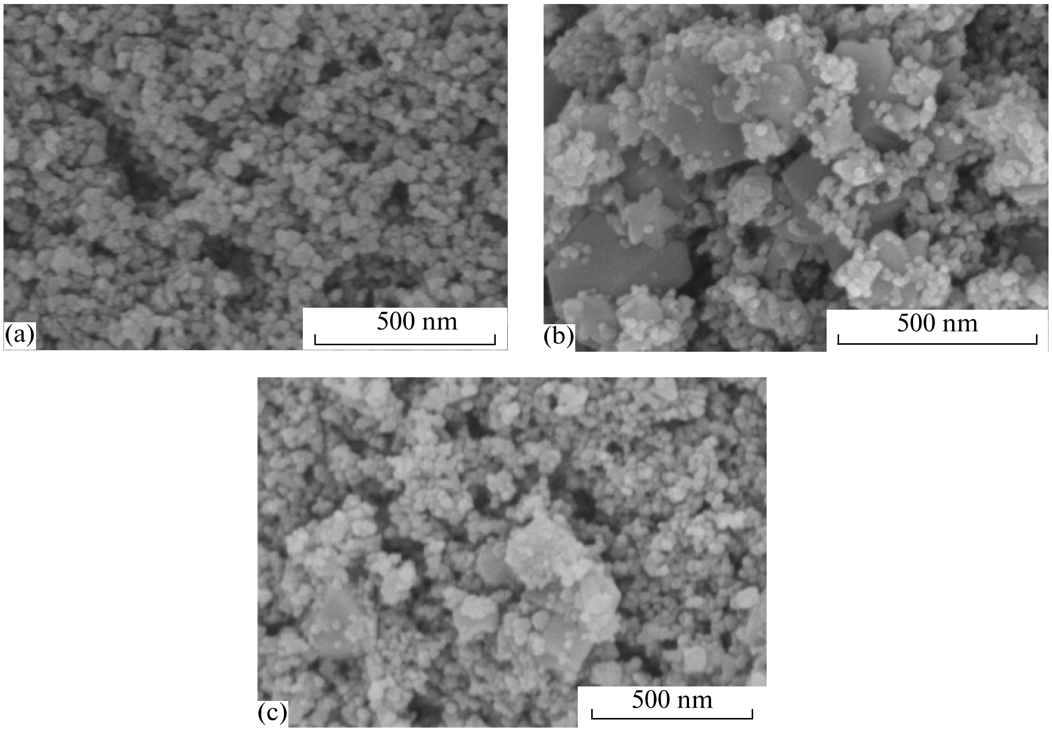

Fig. 6. SEM images of TiO_2 films with 30-nm scattering particles (a), 250-nm scattering particles (b), and mixture of 30-nm and 250-nm TiO_2 particles (c).

tocurrent of the DSSCs ismaximal. The structure (S/N/FTO) with the 250-nm TiO_2 layer for light-scattering obtains a higher J_{sc} than does the structure (N/FTO) with the 30-nm TiO_2 layer. However, V_{oc} decreases slightly. The structure (S/FTO) with the 250-nm TiO_2 layer has the lowest J_{sc}. Due to the enhancement in J_{sc}, significantly higher power conversion efficiencies of the DSSCs were observed, resulting from the scattering properties of TiO_2 films which have light capture inside the device. Consequently, the highest conversion efficiency of 6.7% was obtained for the DSSCs with a TiO_2 electrode structure using an admixture of 30-nm particles and 250-nm particles for the light-scattering layer and 30-nm TiO_2 layer for the dense layer.

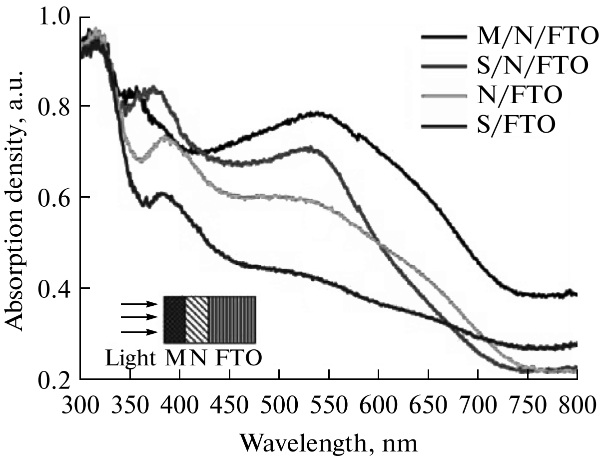

Fig. 7. UV-Vis absorption spectra of the four type TiO_2 films with dye sensitization. N: nanometer-size TiO_2 layer; S: submicron-size TiO_2 layer; M: mixture of submicron- and nanometer-size TiO_2 layer.

CONCLUSIONS

The present study introduces step-by-step procedures to follow in producing screen-printing pastes used to form TiO_2 electrodes used in DSSCs, and investigates the effects of different treatments of TiO_2 electrodes on photovoltaic characteristics of DSSCs. First, $TiCl_4$ treatment on TiO_2 electrodes can produce improvements on the DSSC performance. This effect is caused by reducing charge recombination, enhancing the necking between TiO_2 particles, minimizing the recombination rate between the TiO_2 film and the mediator, and improving electrical contiguity at the FTO/TiO_2 interface. Secondly, photovoltaic performances of DSSCs are improved using HNO_3-treated TiO_2 electrodes. The HNO3 treatment significantly enhances the dispersion of TiO_2 particles and enlarges the surface area and increases porosity of TiO_2 films. Finally, the scattering layer formed by admixing nanometer-sized and submicron-sized TiO_2 particles greatly enhances the DSSC performance. A dye-sensitized TiO_2

film with an admixture of about 20% 30-nm particles and about 80% 250-nm particles demonstrates the optimal integrated absorption intensity. Consequently, the best conversion efficiency of 7.2% was obtained for DSSCs using an admixture light-scattering layer. Light absorption is effectively enhanced in the nanocrystalline film with a mixture of large and small particles, and this mixture is capable of efficient light-scattering while simultaneously providing a larger surface area for effective dye adsorption.

ACKNOWLEDGMENTS

The authors are expressing their gratitude to the National Natural Science Foundation of China (project no. 61076055), the Zhejiang Provincial Science and Technology Key Innovation Team (project no. 2011R 50012) and the Zhejiang Provincial Key Laboratory (project no. 2013 E10022) for their overall support of the present research.

REFERENCES

1. O'Regan, B. and Grätzel, M., A low-cost, high-efficiency solar cell based on dye-sensitized colloidal TiO_2 films, *Nature*, 1991, vol. 353, no. 24, pp. 737–740.
2. Grätzel, M., Photoelectrochemical cells, *Nature*, 2001, vol. 414, no. 6861, pp. 338–343.
3. Bach, U., Lupo, D., Comte, P., Moser, J.E., Weissörtel, F., Salbeck, J., Spreitzert, H., and Grätzel, M., Photochemistry: Solid-state organic solar cells, *Nature*, 1998, vol. 395, no. 6702, pp. 544–545.
4. Krebs, F.C. and Biancardo, M., Dye sensitized photovoltaic cells: attaching conjugated polymers to zwitterionic ruthenium dyes, *Sol. Energy Mater. Sol. Cells*, 2006, vol. 90, no. 2, pp. 142–165.
5. Wang, Z.S., Kawauchi, H., Kashima, T., and Arakawa, H., Significant influence of TiO_2 photoelectrode structure on the energy conversion efficiency of N719 dye-sensitized solar cell, *Coord. Chem. Rev.,* 2004, vol. 248, pp. 1381–1389.
6. Yang, L., Lin, Y., Jia, J., Xiao, X., Li, X., and Zhou, X., Light harvesting enhancement for dye-sensitized solar cells by novel anode containing cauliflower-like TiO_2 spheres, *J. Power Sources*, 2008, vol. 182, no. 1, pp. 370–376.
7. Hore, S., Vetter, C., Kern, R., Smit, H., and Hinsch, A., Influence of scattering layers on efficiency of dye-sensitized solar cells, *Sol. Energy Mater. Sol. Cells*, 2006, vol. 90, no. 9, pp. 1176–1188.
8. Lin, Y., Ma, Y.T., Yang, L., Xiao, X.R., Zhou, X.W., and Li, X.P., Computer simulations of light scattering and mass transport of dye-sensitized nanocrystalline solar cells, *J. Electroanal. Chem.*, 2006, vol. 588, no. 1, pp. 51–58.
9. Ferber, J. and Luther, J., Computer simulations of light scattering and absorption in dye-sensitized solar cells, *Sol. Energy Mater. Sol. Cells*, 1998, vol. 54, nos. 1–4, pp. 265–275.
10. Barbe, C.J., Arendse, F., and Comte, P., Nanocrystalline titanium oxide electrodes for photovoltaic applications, *J. Am. Ceram. Soc.*, 1997, vol. 80, no. 12, pp. 3157–3171.
11. Nazeeruddin, M.K., Kay, A., Rodicio, I., Humphry-Baker, R., Müller, E., Liska, P., Vlachopoulos, N., and Grätzel, M., Conversion of light to electricity by *cis*-X2bis(2,2'-bipyridyl-4,4'-dicarboxylate) ruthenium(II) charge-transfer sensitizers ($X = Cl^-$, Br^-, I^-, CN^-, and SCN^-) on nanocrystalline titanium dioxide electrodes, *J. Am. Chem. Soc.,* 1993, vol. 115, no. 14, pp. 6382–6390.
12. Ito, S., Liska, P., Comte, P., Charvet, R., Péchy, P., Bach, U., Schmidt-Mende, L., Zakeeruddin, S.M., Kay, A., Nazeeruddin, M.K., and Grätzel, M., Control of dark current in photoelectrochemical ($TiO_2/I^- - I_3^-$) and dye-sensitized solar cells, *Chem. Comm.*, 2005, vol. 34, pp. 4351–4353.
13. O'Regan, B.C., Durrant, J.R., Sommeling, P.M., and Bakker, N.J., Influence of the $TiCl_4$ treatment on nanocrystalline TiO_2 films in dye-sensitized solar cells. 2: Charge density, band edge shifts, and quantification of recombination losses at short circuit, *J. Phys. Chem., Ser. C,* 2007, vol. 111, pp. 14001–14010.
14. Kambe, S., Nakade, S., Wada, Y., Kitamura, T., and Yanagida, S., Effects of crystal structure, size, shape and surface structural differences on photo-induced electron transport in TiO_2 mesoporous electrodes, *J. Mater. Chem.*, 2002, vol. 12, no. 3, pp. 723–728.
15. Wang, Z., Yamaguchi, T., Sugihara, H., and Arakawa, H., Significant efficiency improvement of the black dye-sensitized solar cell through protonation of TiO_2 films, *Langmuir,* 2005, vol. 21, no. 21, pp. 4272–4276.
16. Ito, S., Kitamura, T., Wada, Y., and Yanagida, S., Facile fabrication of mesoporous TiO_2 electrodes for dye solar cells: chemical modification and repetitive coating, *Sol. Energy Mater. Sol. Cells,* 2003, vol. 76, no. 1, pp. 3–13.
17. Jung, H.S., Lee, J., Lee, S., Hong, K.S., and Shin, H., Acid adsorption on TiO_2 nanoparticles an electrochemical properties study, *J. Phys. Chem., Ser. C*, 2008, vol. 112, no. 22, pp. 8476–8480.
18. Hao, S., Wu, J., Fan, L., Huang, Y., Lin, J., and Wei, Y., The influence of acid treatment of TiO_2 porous film electrode on photoelectric performance of dye-sensitized solar cell, *Sol. Energy*, 2004, vol. 76, no. 6, pp. 745–750.
19. *Semiconductor Electrodes,* Finklea, H.O., Ed., Amsterdam: Elsevier, 1988, p. 520.
20. Musić, S., Gotić, M., Ivanda, M., Popović, S., Turković, A., Trojko, R., Sekulić, A., and Furić, K., Chemical and micro structural properties of TiO_2 synthesized by sol–gel procedure, *Mater. Sci. Eng., Ser. B*, 1997, vol. 47, no. 1, pp. 33–40.
21. Sommeling, P.M., O'Regan, B.C., Haswell, R.R., Smit, H.J.P., Bakker, N.J., Smits, J.J.T., Kroon, J.M., and van Roosmalen, J.A.M., Influence of a $TiCl_4$ post-treatment on nanocrystalline TiO_2 films in dye-sensitized solar cells, *J. Phys. Chem., Ser. B*, 2006, vol. 110, no. 399, p. 19191.
22. Jung, H.S., Lee, J., Nastasi, M., Lee, S., Kim, J., Park, J., Hong, K.S., and Shin, H., Preparation of nano-porous MgO-coated TiO_2 nanoparticles and their application to the electrode of dye-sensitized solar cells, *Langmuir*, 2005, vol. 21, no. 23, pp. 10332–10335.
23. Redmond, G. and Fitzmaurice, D., Spectroscopic determination of flatband potentials for polycrystalline titania electrodes in nonaqueous solvents, *J. Phys. Chem.,* 1993, vol. 97, no. 7, pp. 1426–1430.